ARCHIVE OF MECHANICAL ENGINEERING

DOI: 10.24425/ame.2025.155871 2025, Vol. 72, No. 4, pp. 563–582

Shubham BANSAL [1,2], Rajendra Singh YADAV [1], Ankita ANKITA [3], Oluwole Daniel MAKINDE [4]

Unsteady MHD mixed convective flow over a permeable stretching cylinder: impact of curvature, velocity slip, and thermal conductivity variations

Received 13 July 2025, **Revised** 30 August 2025, **Accepted** 19 September 2025, **Published online** 17 October 2025

Keywords: unsteady flow, slip velocity, mixed convection, variable thermal conductivity

This paper presents a numerical investigation of unsteady, two-dimensional magnetohydrodynamic (MHD) mixed convection flow and heat transfer over a permeable stretching cylinder embedded in a porous medium. The governing conservation equations of mass, momentum, and energy are formulated by incorporating the effects of viscous dissipation, temperature-dependent thermal conductivity, Joule heating, thermal radiation, and a uniform transverse magnetic field (with negligible induced effects). Additionally, slip velocity and variable surface heat flux are also considered to enhance the model's applicability to engineering systems. Through appropriate similarity transformations, the governing partial differential equations are reduced to a set of nonlinear ordinary differential equations, which are solved using MATLAB's bvp4c scheme. The influence of key dimensionless parameters on velocity and temperature distributions, skin friction coefficient, and Nusselt number is thoroughly examined. Comparative analysis between the stretching cylinder and the flat sheet configurations reveals that the cylinder's curvature significantly thickens the momentum and thermal boundary layers, while enhancing the surface shear stress and heat transfer rate. These findings offer useful implications for the design of thermal systems involving curved geometries, such as cylindrical heat exchangers and pipes.

✉ Rajendra Singh Yadav, email: rajendrauor@gmail.com

[1]Department of Mathematics, University of Rajasthan, Jaipur, Rajasthan-302004, India

[2]SBD Government College, Sardarshahar, Churu, Rajasthan-331403, India

[3]Department of Physics, Government Girls College, Taranagar, Rajasthan-331304, India

[4]Faculty of Military Science, Stellenbosch University, Saldanha, South Africa

Nomenclature

a	positive constant (s^{-1})	Nu_x	Nusselt number
A_1	constant (Kg/s^3)	Pr	Prandtl number
B	magnetic field (Tesla)	$Q(>0$ or $<0)$	heat source/sink coefficient
b	characteristic velocity (m/s)	Q_0	constant
B_0	constant (Tesla)	q_r	radiative heat flux (Kg/m^2)
B_1	velocity slip coefficient (s/m)	$q_w(x,t)$	surface heat flux (Kg/s^3)
c_p	specific heat (m^2/s^2K)	R	radius of the cylinder
Cf_x	skin-friction coefficient	Re_x	Reynols number
f	non-dimensional stream function	T	fluid temperature (K)
g	gravitational acceleration (m/s^2)	t	time (s)
k^*	absorption coefficient	T_∞	ambient temperature of the fluid (K)
k_0	constant (m^2)	$U_w(x,t)$	stretching velocity of the cylinder (m/s)
k_p	permeability of porous medium (m^2)	x, r	cylindrical coordinates
L	characteristic length (m)		

Greek symbols

β_0	thermal expansion coefficient (K^{-1})	ψ	stream function
ϵ	thermal conductivity parameter	ρ	fluid density (Kg/m^3)
$\grave{u}, \grave{v}$	velocity components (m/s)	σ	electrical conductivity (S/m)
κ	thermal conductivity (Kgm/s^3K)	σ^*	Stefan-Boltzman constant
κ_∞	ambient thermal conductivity (Kgm/s^3K)	θ	non-dimensional temperature
μ	fluid viscosity (Kg/m s)	ζ	dimensionless variable
ν	kinematic viscosity (m^2/s)		

List of abbreviations

2-D	Two-dimensional	ODE	Ordinary differential equation
MHD	Magnetohydrodynamic	FDM	Finite difference method
BLF	Boundary layer flow	BVP	Boundary value problem
TP	Temperature profile	IVP	Initial value problem
MBL	Momentum boundary layer	VP	Velocity profile
VHF	Variable heat flux	TBL	Thermal boundary layer
PDE	Partial differential equation		

1. Introduction

The investigation of Newtonian fluid flow over a stretching surface is crucial in theoretical fluid mechanics and various industrial applications, including polymer extrusion, glass manufacturing, and the cooling of metallic sheets. Newtonian fluids, characterized by constant viscosity that remains independent of applied shear stress, demonstrate distinct boundary layer behavior when subjected to uniformly stretching surfaces. The problem of fluid flow over a stretching surface was first examined by Crane [1], who introduced the concept of a linearly stretching sheet

in his pioneering work. Furthermore, fluid flow and heat transfer over a stretching cylinder have numerous engineering applications, including cylindrical heat pipes, biosensors, pipe fabrication, and food processing. Wang [2] was the pioneer in analyzing this flow configuration. Since then, numerous studies have been conducted on stretching cylinders under the effect of various governing parameters to highlight their industrial relevance. Ishak et al. assessed MHD [3] and suction/blowing effect [4]; Mukhopadhyay and Gorla [5] examined slip effects; Vajravelu et al. [6] considered variable properties and heat sources/sinks; Munawar et al. [7] addressed unsteady prescribed and variable heat flux; Poply et al. [8] evaluated thermal radiation; Mehdy [9] studied Joule heating and viscous dissipation; and Mukhopadhyay [10] investigated mixed convection effect in porous media.

Magnetohydrodynamic (MHD) flow is significant for controlling electrically conducting fluids using magnetic fields, with applications in power generation, metal processing, aerospace systems, and boundary layer management [11]. Elbashbeshy et al. [12] studied boundary layer flow (BLF) over a stretching cylinder and found that a stronger magnetic field reduces velocity while increasing the temperature profile (TP). Viscous dissipation and Joule heating act as internal heat sources that significantly influence TP and heat transfer in conducting fluids. Swain et al. [13] investigated MHD flow and heat transfer over a stretching sheet in a porous medium, highlighting that increased viscous dissipation and Joule heating elevate fluid temperature and thermal boundary thickness. Their findings are relevant to applications in heating systems, polymer processing, and food industries. Kumar et al. [14] studied Williamson fluid flow over a permeable stretching cylinder, emphasizing that viscous dissipation and Joule heating significantly affect temperature and heat transfer. Sinha et al. [15] investigated MHD flow of Jeffrey fluid over a wedge using the Keller-Box method, showing that viscous dissipation and Joule heating notably affect temperature and heat transfer characteristics. Khan et al. [16] studied MHD flow over a stretching cylinder with thermal radiation, revealing that suction/blowing notably affects flow and heat transfer, which is crucial in boundary layer control applications like film cooling and fiber coating.

Most of the above studies focus on steady flows. Megahed et al. [17] examined unsteady flow over a stretching surface with variable fluid properties and heat flux, finding that the unsteadiness parameter reduces boundary layer temperature. Similarly, Khan et al. [18] analyzed unsteady stretching sheet flow with thermal radiation and viscous dissipation in a porous medium, highlighting its effect on thermal behavior. Qayyum et al. [19] studied unsteady hybrid nanofluid flow between rotating stretching disks, highlighting the impact of convective boundaries on heat and mass transfer. Megahed [20] studied Carreau fluid flow over a nonlinear sheet, showing that variable thermal conductivity reduces surface temperature and affects heat transfer. Variable thermal conductivity significantly influences heat transfer performance, particularly in temperature-dependent fluid flows. Waseem et al. [21] analyzed the flow of hybrid nanofluid over a nonlinear stretching surface, highlighting that an increase in the thermal conductivity parameter enhances the

system's heat as well as the Nusselt number. Numerous studies have explored its effects on different geometries and flow conditions to enhance the accuracy of thermal analysis [22–26].

Mixed convection, arising from the combined effects of buoyancy and forced flow, has vital applications in numerous fields such as solar energy systems, electronics cooling, nuclear reactor safety, heat exchangers, and building ventilation. It also plays a key role in environmental and geophysical processes like atmospheric and oceanic flows [27]. Several researchers have analyzed the impact of mixed convection on BLF under different physical scenarios. Ismail et al. [28] showed that magnetic fields influence unsteady mixed convection flow over a cylinder by delaying flow separation. Lim et al. [29] reported that increasing the mixed convection parameter thickens the momentum boundary layer (MBL), reducing skin friction. Abbas et al. [30] found that it enhances velocity while lowering temperature in Williamson fluid flow over a stretched cylinder.

Velocity slip, a deviation from the classical no-slip condition, occurs when fluid near a solid boundary does not match the surface velocity. This phenomenon plays a crucial role in enhancing flow behavior and heat transfer, with applications in biomedical devices like artificial heart valves, precision manufacturing techniques, and tribological systems such as engines and bearings. Tamoor [31] showed that slip affects both velocity and temperature profiles over a nonlinearly stretching cylinder. Das et al. [32] found that slip reduces shear stress and heat transfer in radiative flow over a vertical cylinder. Recently, Bansal and Yadav [33] reported that increasing slip decreases skin friction and Nusselt number while enhancing temperature in porous media flow. Several studies have explored the influence of velocity slip on flow and heat transfer characteristics, including the works of Nandeppanavar et al. [34] on a moving plate, Cham and Mustafa [35] on viscoelastic fluid, and Ullah et al. [36] on Casson fluid over a stretching cylinder.

Curvature significantly influences boundary layer behavior, with cylindrical surfaces exhibiting distinct flow and heat transfer characteristics compared to flat geometries. An increase in curvature typically enhances thermal gradients and modifies skin friction. Sadighi et al. [37] investigated MHD flow over a permeable stretching cylinder and observed that curvature notably increases the skin friction coefficient and Nusselt number compared to a stretching sheet. Similarly, Reddy et al. [38] reported that a higher curvature parameter strengthens the temperature gradient in the boundary layer around the cylinder. Several researchers have conducted comparative studies on flow and heat transfer over stretching sheets and cylinders by varying the curvature parameter [39–41].

Although several studies have addressed boundary layer flow and heat transfer over stretching surfaces, a detailed and unified analysis incorporating multiple physical phenomena for cylindrical configurations is still limited. The present work offers a comprehensive investigation by simultaneously accounting for the effects of magnetic field, mixed convection, porous medium, viscous dissipation, Joule heating, thermal radiation, unsteadiness, temperature-dependent thermal conductivity,

heat source/sink, velocity slip, suction/blowing, and variable heat flux. Notably, very few studies consider unsteady flow with variable thermal conductivity over a stretching cylinder, and comparative studies between flat and curved surfaces under identical physical scenarios are rarely explored.

The novelty of this study lies in its extensive comparative analysis of fluid flow over both stretching sheets and cylinders under the influence of a wide range of realistic physical parameters. This enables a deeper understanding of how surface curvature affects momentum and thermal boundary layers, skin friction, and heat transfer performance. The outcomes are expected to contribute significantly to the design of advanced thermal systems involving curved geometries, such as in polymer extrusion, wire coating, and cooling of cylindrical electronic components.

2. Mathematical formulation

2.1. Flow description

In this problem, we consider an unsteady, axisymmetric, 2-D boundary layer laminar flow of viscous incompressible electrically conducting fluid due to a permeable stretching cylinder of radius 'R' aligned along the x-axis. We assume a coordinate system (x, r), where the x-axis is aligned with the cylinder's axis and the r-axis extends radially outward (see Fig. 1). The flow is driven by the stretching of the cylinder surface with a velocity

$$U_w(x,t) = \frac{bx}{L(1-at)}. \tag{1}$$

As a result, a momentum boundary layer develops along the radial direction. Simultaneously, thermal effects induce a thermal boundary layer adjacent to the surface. In the present study, we made the following assumptions:

- Newtonian fluid model is considered.
- Viscous dissipation, thermal radiation, Joule heating, heat source/sink effect with $Q = \dfrac{Q_0}{(1-at)}$ are employed in the energy equation.
- Flow is considered within a porous medium with permeability $k_p(t) = k_0(1-at)$.
- The impact of slip velocity and variable heat flux is taken at the boundary.
- A uniform magnetic field $B = B_0$ applied in the radial direction, while the effects of the induced magnetic field are disregarded.
- The fluid's thermophysical properties are considered constant, except for thermal conductivity, which depends on temperature in the energy equation, and density variations that introduce a buoyant force term in the momentum equation.

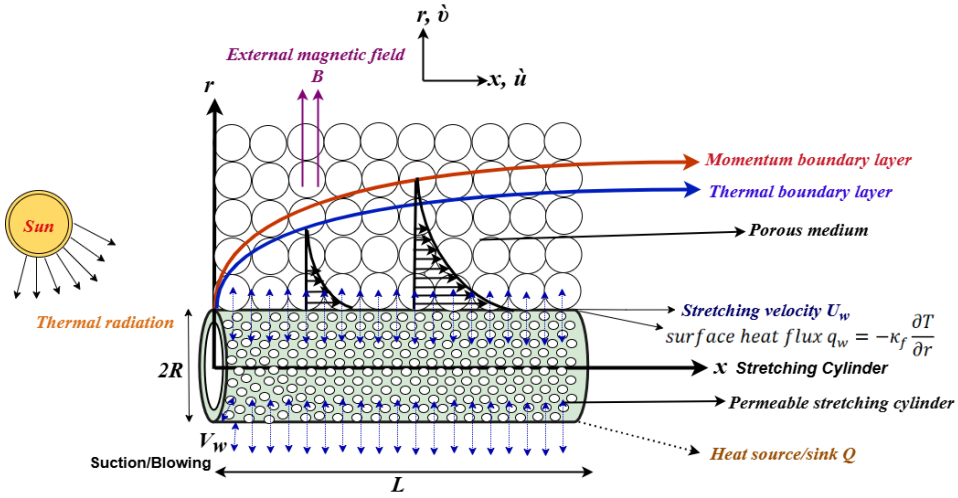

Fig. 1. Flow model of the problem

2.2. Governing equations

Using Boussinesq approximation, the governing equations (mass, momentum, and energy conservation) for the present problem are [22, 24, 37, 42]:

$$\frac{\partial(r\grave{u})}{\partial x} + \frac{\partial(r\grave{v})}{\partial r} = 0, \tag{2}$$

$$\frac{\partial \grave{u}}{\partial t} + \grave{u}\frac{\partial \grave{u}}{\partial x} + \grave{v}\frac{\partial \grave{u}}{\partial r} = \frac{\mu}{\rho}\left(\frac{\partial^2 \grave{u}}{\partial r^2} + \frac{1}{r}\frac{\partial \grave{u}}{\partial r}\right) - \frac{\mu}{\rho k_p}\grave{u} - \frac{\sigma B^2}{\rho}\grave{u} + g\beta_0(T - T_\infty), \tag{3}$$

$$\frac{\partial T}{\partial t} + \grave{u}\frac{\partial T}{\partial x} + \grave{v}\frac{\partial T}{\partial r} = \frac{1}{\rho c_p}\frac{1}{r}\frac{\partial}{\partial r}\left(\kappa(T) r \frac{\partial T}{\partial r}\right) + \frac{\mu}{\rho c_p}\left(\frac{\partial \grave{u}}{\partial r}\right)^2 - \frac{1}{\rho c_p}\frac{\partial q_r}{\partial y} + \frac{\sigma B^2}{\rho c_p}\grave{u}^2 + \frac{\mu}{\rho c_p k_p}\grave{u}^2 + \frac{Q}{\rho c_p}(T - T_\infty). \tag{4}$$

The relevant boundary conditions are:

$$\grave{u} = U_w + B_1 \nu \frac{\partial \grave{u}}{\partial r}, \quad \grave{v} = V_w, \quad q_w = -\kappa\frac{\partial T}{\partial r} = A_1\left(\frac{x}{L}\right)^2 \frac{1}{(1-at)^{5/2}}, \quad \text{at} \quad r = R, \tag{5}$$

$$\grave{u} \to 0, \quad T \to T_\infty \quad \text{as} \quad r \to \infty. \tag{6}$$

Where $B_1 = B_1'\sqrt{(1-at)}$ is the slip velocity coefficient and q_w is the VHF on the surface, which varies with distance x and time t, A_1 is the constant wall heat flux, $\grave{u}$ and $\grave{v}$ are velocity components in x and r-directions, σ represents electrical conductivity, κ represents thermal diffusivity and μ is the viscosity of the fluid.

In this model, the radiative heat flux q_r is given by Rosseland approximation assuming temperature as a linear function [43]:

$$q_r = -\frac{16\sigma^* {T_\infty}^3}{3k^*}\frac{\partial T}{\partial r}. \tag{7}$$

The fluid's thermal conductivity is assumed to have a linear variation with temperature, expressed as [22]:

$$\kappa = \kappa_\infty(1+\epsilon\theta), \tag{8}$$

where ϵ is the thermal conductivity parameter.

2.3. Similarity transformations

To solve the governing PDEs (2)-(4) with boundary conditions (5)-(6), we use the following transformations:

$$\zeta = \frac{r^2-R^2}{2R}\left(\frac{b}{\nu L(1-at)}\right)^{\frac{1}{2}}, \quad \psi(x,r) = \left(\frac{b\nu}{L(1-at)}\right)^{\frac{1}{2}} xRf(\zeta), \tag{9}$$

$$T = T_\infty + \frac{q_w}{\kappa_\infty}\sqrt{\frac{\nu L(1-at)}{b}}\theta(\zeta). \tag{10}$$

Where ζ is the similarity variable, and $f(\zeta)$ and $\theta(\zeta)$ are the dimensionless stream function and temperature. The dimensional stream function is $\psi(x,r)$ which identically satisfies the continuity equation with $\grave{u} = \frac{1}{r}\frac{\partial\psi}{\partial r}$, $\grave{v} = -\frac{1}{r}\frac{\partial\psi}{\partial x}$. The governing PDEs (2)-(4) are reduces into non-linear dimensionless ODEs as

$$(1+2\delta\zeta)f''' + 2\delta f'' + ff'' - f'^2 - S\left(f' + \frac{\zeta}{2}f''\right) - (\mathrm{Ha}+\mathrm{Da})f' + \beta\theta = 0, \tag{11}$$

$$(1+Rd+\epsilon\theta)(1+2\delta\zeta)\theta'' + [2(1+\epsilon\theta)+Rd]\,\delta\theta' + (1+2\delta\zeta)\epsilon\theta'^2 + \mathrm{Pr}\left[(f\theta' - 2f'\theta) - S\left(2\theta + \frac{\zeta}{2}\theta'\right) + \mathrm{Ec}(1+2\delta\zeta)f''^2 + \mathrm{Ec}(\mathrm{Ha}+\mathrm{Da})f'^2 + \gamma\theta\right] = 0. \tag{12}$$

The reduced boundary conditions are:

$$f(0) = s, \quad f'(0) = 1+\lambda f''(0), \quad \theta'(0) = \frac{-1}{1+\epsilon\theta(0)}, \quad \text{at} \quad \zeta = 0, \tag{13}$$

$$f'(\zeta) \to 0, \quad \theta(\zeta) \to 0 \quad \text{as} \quad \zeta \to \infty. \tag{14}$$

The dimensionless paraeters appearing in Eqs. (11)–(14) are summarized in Table 1.

Table 1. Dimensionless parameters

Velocity slip parameter	$\lambda = B_1'\sqrt{\frac{b\nu}{L}}$	Darcy number	$\mathrm{Da} = \frac{\mu L}{\rho k_0 b}$
Curvature parameter	$\delta = \sqrt{\frac{\nu L(1-at)}{bR^2}}$	Radiation parameter	$Rd = \frac{16\sigma^* {T_\infty}^3}{3\kappa_\infty k^*}$
Heat source/sink parameter	$\gamma = \frac{Q_0 L}{\rho c_p b}$	Eckert number	$\mathrm{Ec} = \frac{U_w^2}{c_p(T_w - T_\infty)}$
Unsteadiness parameter	$S = \frac{aL}{b}$	Hartmann number	$\mathrm{Ha} = \frac{\sigma {B_0}^2 L(1-at)}{b\rho}$
Suction/blowing parameter	$s = -V_w\sqrt{\frac{L(1-at)}{b\nu}}$	Prandtl number	$\mathrm{Pr} = \frac{\mu c_p}{\kappa_\infty}$
Mixed convection parameter	$\beta = \frac{\mathrm{Gr}_x}{\mathrm{Re}_x^2}$	Grashof number	$\mathrm{Gr}_x = g\beta_0(T_w - T_\infty)\frac{x^3}{\nu^2}$

2.4. Physical quantities

To determine the flow behavior and heat transfer characteristics, the vital physical quantities having engineering application are the coefficient of skin friction (Cf_x) and Nusselt number (Nu_x) given as [37]:

$$Cf_x = \frac{\tau_w}{\rho {U_w}^2}, \quad \mathrm{Nu}_x = \frac{x q_w}{\kappa_\infty (T_w - T_\infty)}, \tag{15}$$

where $\tau_w = \left(\mu \frac{\partial \grave{u}}{\partial r}\right)_{r=R}$ is the surface shear stress and $q_w(x,t) = \left(-\kappa \frac{\partial T}{\partial r} + q_r\right)_{r=R}$ is the surface heat flux.

Now, introducing Eqs. (9)–(10) in Eq.(15), the dimensionless form of the Cf_x and Nu_x for the present problem is

$$Cf_x \mathrm{Re}_x^{1/2} = f''(0), \qquad \mathrm{Nu}_x \mathrm{Re}_x^{-1/2} = \left(1 + \frac{Rd}{1 + \epsilon\theta(0)}\right)\frac{1}{\theta(0)}. \tag{16}$$

3. Method of solution

3.1. Numerical method

The highly nonlinear momentum and energy equations (PDEs) from Eq. (3)–(4) with boundary conditions (5)–(6) are transformed into a system of ODEs, given by Eq. (11)–(12) with boundary conditions (13)–(14). Due to the strong nonlinearity and coupled nature of these equations, obtaining an exact analytical solution is not feasible. Therefore, the MATLAB built-in numerical solver bvp4c is employed to obtain the solution, and the corresponding flow chart of the numerical procedure is shown in Fig. 2. This solver, which utilizes a collocation

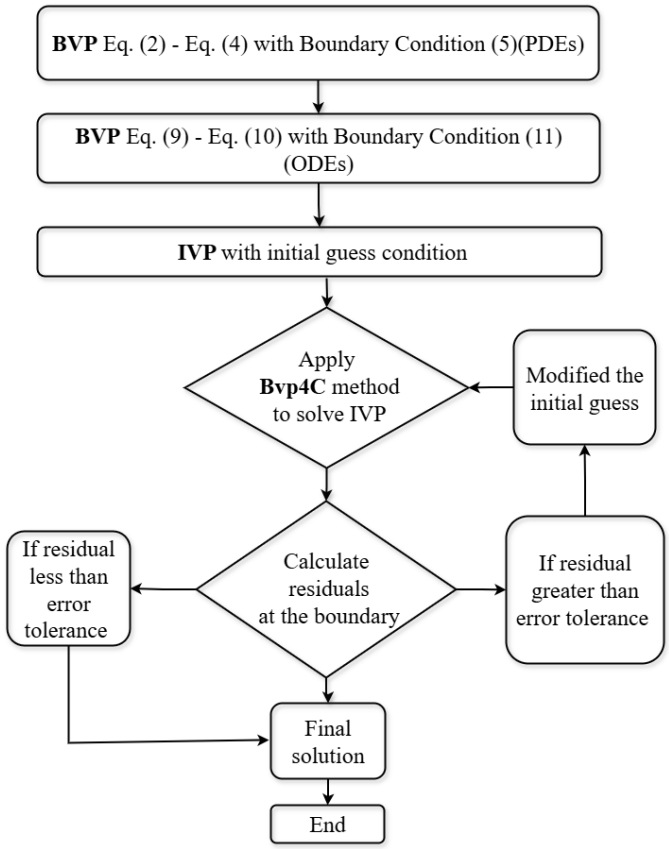

Fig. 2. Flow chart of numerical method

method based on the finite difference approach and the Lobatto IIIa formula, ensures fourth-order accuracy while automatically refining the computational mesh to resolve steep gradients effectively. One key advantage of bvp4c is its ability to handle stiff, nonlinear boundary value problems without requiring initial guesses for the missing boundary conditions, which often complicate shooting methods. Additionally, its adaptive mesh adjustment improves solution accuracy near boundary layers compared to traditional finite difference or finite element techniques with fixed grids. To implement this method, the original boundary value problem is converted into a system of first-order ordinary differential equations by introducing suitable auxiliary variables:

$$Z_1 = f(\zeta), \quad Z_2 = f'(\zeta), \quad Z_3 = f''(\zeta), \quad Z_4 = \theta(\zeta), \quad Z_5 = \theta'(\zeta). \tag{17}$$

Then the system of IVP:

$$Z_1' = Z_2, \qquad Z_1(0) = s,$$
$$Z_2' = Z_3, \qquad Z_2(0) = 1 + \lambda Z_3(0),$$

$$Z_3' = \frac{1}{(1+2\delta\zeta)}\left[Z_2^2 + S\left(Z_2 + \frac{\zeta}{2}Z_3\right) + (\mathrm{Ha}+\mathrm{Da})Z_2 - 2\delta Z_3 - Z_1 Z_3 - \beta Z_4\right], \quad (18)$$

$$Z_3(0) = S_{01},$$

$$Z_4' = Z_5, \qquad Z_4(0) = S_{02},$$

$$Z_5' = \frac{1}{(1+Rd+\epsilon Z_4)(1+2\delta\zeta)}\left[\mathrm{Pr}\left(2Z_2Z_4 - Z_1Z_5 + S\left(2Z_4 + \frac{\zeta}{2}Z_5\right) - \mathrm{Ec}(1+2\delta\zeta){Z_3}^2 - \mathrm{Ec}(\mathrm{Ha}+\mathrm{Da}){Z_2}^2 - \gamma Z_4\right) - (2(1+\epsilon Z_4)+Rd)\,\delta Z_5 - (1+2\delta\zeta)\epsilon {Z_5}^2\right], \qquad Z_5(0) = -\frac{1}{1+\epsilon Z_4(0)},$$

and additional conditions

$$Z_2(\infty) = 0, \quad Z_4(\infty) = 0. \quad (19)$$

Now, suitable initial guesses $Z_3(0) = S_{01}$ and $Z_4(0) = S_{02}$ for the missing boundary conditions are made to ensure the system is integrated correctly. The numerical integration extends over an interval [0,15], where =15 with step size 0.01 to ensure the boundary conditions are satisfied asymptotically.

3.2. Validation of method

In this section, To ensure the accuracy of the numerical method using the bvp4c solver, the results were compared to the exact solutions obtained by Sina Sadighi et al. [37] using the confluent hypergeometric function. The comparison was conducted for various δ values of $-f''(0)$ and $\frac{1}{\theta(0)}$, keeping the parameters $s = -30, \mathrm{Ha} = 1, \mathrm{Pr} = 8, Rd = 1, \gamma = -1$, $\mathrm{Da} = 0.5$, and $\mathrm{Ec} = 1$ consistent with their study [37] while ignoring the parameters $\lambda = \beta = S = \epsilon = 0$, as shown in Table 2. The results matched up to six decimal places, confirming the precision and reliability of the bvp4c solver to solve complex nonlinear differential equations. This high level of agreement validates the numerical approach and demonstrates that the method can accurately capture the system's behavior, even when compared to exact solutions.

Table 2. Comparison of $-f''(0)$ and $\frac{1}{\theta(0)}$ values with Sadighi et al.[37] when $s = -30$, $\mathrm{Pr} = 8$, $\mathrm{Ha} = 1$, $Rd = 1$, $\gamma = -1$, $\mathrm{Ec} = 1$, $\mathrm{Da} = 0.5$, $S = \lambda = \epsilon = \beta = 0$ for different values of δ

δ	Sadighi et al. [37]		Current work	
	$-f''(0)$	$\frac{1}{\theta(0)}$	$-f''(0)$	$\frac{1}{\theta(0)}$
0.000	0.083103	0.095129	0.083103	0.095129
0.001	0.083108	0.095130	0.083108	0.095130
0.002	0.083114	0.095131	0.083114	0.095131

4. Results and discussion

A comparative analysis has been performed to investigate the influence of various factors in the governing flow equations for the stretching cylinder and sheet. Numerical computations have been carried out to evaluate and illustrate the effects of several physical parameters by varying the non-dimensional quantities: Ha, Da, Ec, $\epsilon, \lambda, \gamma, \delta, Rd, \beta, s, S$ on the flow and heat transfer behavior. The impact of these controlled parameters on VP and TP for the cylinder and sheet is depicted in Figs. (3)–(13).

4.1. Velocity and temperature profile

The geometry of the stretching surface notably influences the VP and TP, as evident from all figures. The curvature parameter δ, which is inversely related to the cylinder's radius, distinguishes the two configurations: $\delta = 0$ for a flat sheet and $\delta = 0.5$ for the stretching cylinder. For the cylinder, the velocity near the surface is initially lower but eventually exceeds that of the sheet farther from the wall due to reduced resistance, resulting in a thicker MBL. A similar trend is observed in TP, where limited surface contact initially reduces heat transfer, but enhanced convection increases the temperature away from the wall.

The influence of Da on VP and TP is illustrated in Figs. 3a and 3b. The lower values of Da corresponds to higher permeability, facilitating easier fluid flow, as expressed by $\mathrm{Da} = \dfrac{\mu L}{b\rho k_0}$. When Da increases, it signifies a reduction in the permeability of the porous medium. This increased flow resistance leads to a decline in the fluid's velocity. As a result, the momentum boundary layer becomes thinner because the fluid attains the free-stream velocity more rapidly. In contrast, when the Darcy number rises, indicating lower permeability, the fluid moves more slowly, allowing for greater heat diffusion from the surface into the fluid which leads to a thicker TBL.

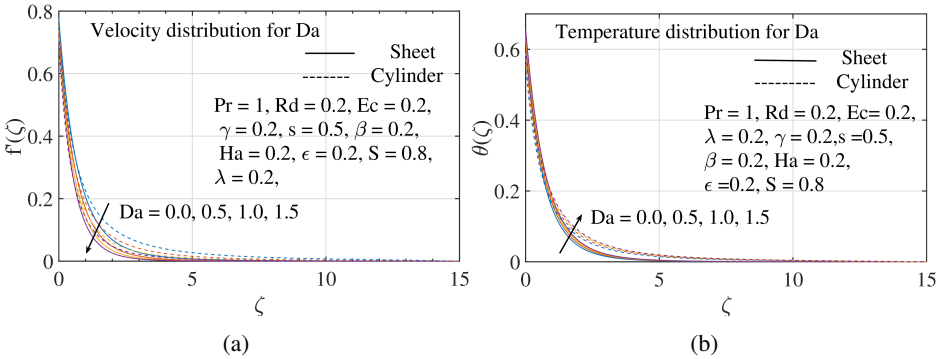

Fig. 3. Impact on (a) velocity and (b) temperature with ζ for different Da

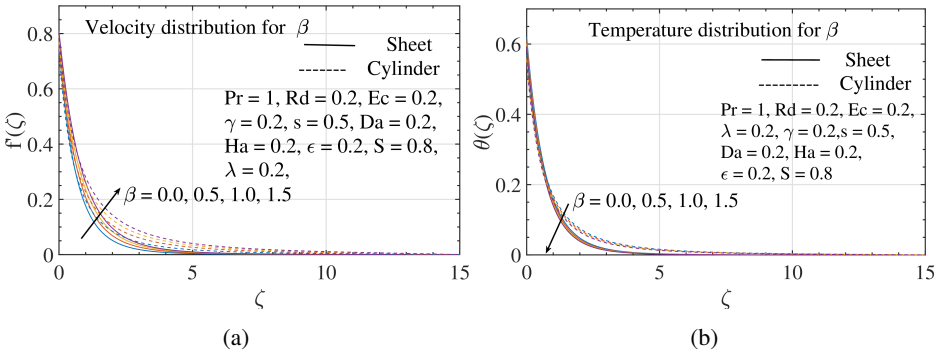

Fig. 4. Impact on (a) velocity and (b) temperature with ζ for different β

The influence of the parameter β on the VP and TP is depicted in Figs. 4a and 4b. An increase in β enhances the velocity profile due to stronger buoyancy forces that induce a favorable pressure gradient, thereby accelerating the flow within the boundary layer and resulting in a thicker MBL. In contrast, the temperature profile diminishes with rising β, leading to a thinner thermal boundary layer owing to the increased temperature gradient near the surface. Consequently, the surface heat transfer rate improves with higher values of β.

The impact of Ha on VP and TP is presented in Figs. 5a and 5b. The interaction between the magnetic field and the conducting fluid generates a Lorentz force that opposes the flow, reducing fluid momentum and leading to a thinner velocity boundary layer. As Ha increases, this magnetic damping effect becomes more significant, causing a notable drop in flow velocity. Additionally, Joule heating raises the temperature within the boundary layer, but the reduced convective flow limits heat transfer efficiency. As a result, TBL becomes thicker, and the Nusselt number decreases.

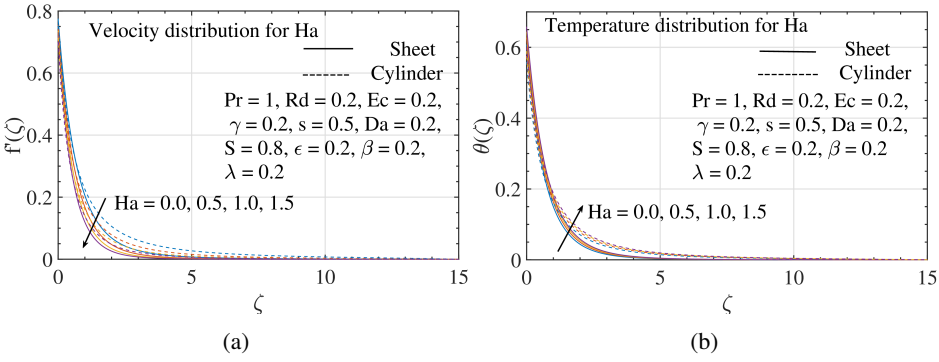

Fig. 5. Impact on (a) velocity and (b) temperature with ζ for different Ha

The effects of the unsteadiness parameter S on the VP and TP are shown in Figs. 6a and 6b. As S increases, both VP and TP decrease due to stronger unsteady

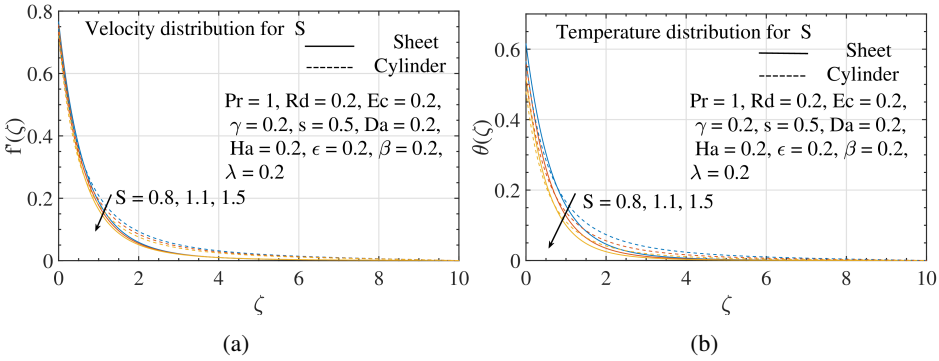

Fig. 6. Impact on (a) velocity and (b) temperature with ζ for different S

effects, leading to thinner velocity and thermal boundary layers. The impact of S is more significant on TP than on VP. Additionally, the surface temperature decreases with higher S, resulting in an increased Nusselt number, indicating better heat transfer. The skin friction coefficient also rises with increasing S, due to steeper velocity gradients near the surface. These effects are crucial for optimizing cooling systems in unsteady flow conditions, such as heat exchangers or manufacturing processes involving moving surfaces.

The influence of λ on both VP and TP leads to noticeable effects that can be seen in Figs. 7a and 7b. As λ increases, the VP decreases due to the diminished friction between the fluid and the stretching surface, which causes the fluid to slip instead of fully adhering to the surface. This results in a thinner MBL, as the fluid's velocity near the surface decreases. On the other hand, the TP increases with increasing λ, as the slip condition weakens the direct interaction between the surface and the fluid, reducing convective heat transfer and allowing more heat to diffuse into the thermal boundary layer. This increase in heat diffusion raises the surface temperature and causes TBL to thicken, which in turn lowers the Nusselt number.

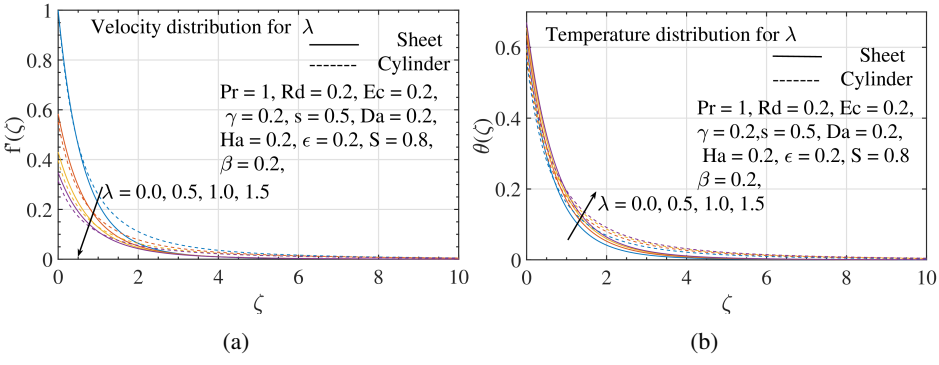

Fig. 7. Impact on (a) velocity and (b) temperature with ζ for different λ

The suction/blowing parameter s has a notable impact on both VP and TP which can be seen in Figs. 8a and 8b. As the suction parameter ($s > 0$) increases, fluid is extracted from the boundary layer, which lowers the velocity near the surface and decreases the VP. Similarly, TP is reduced because suction brings cooler fluid toward the surface, thinning the TBL. In contrast, the blowing parameter $s < 0$ produces the opposite effect.

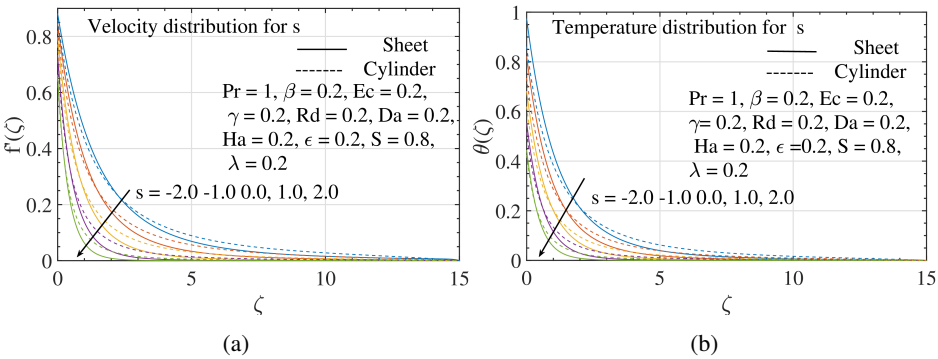

Fig. 8. Impact on (a) velocity and (b) temperature with ζ for different s

The impact of the heat source/sink parameter γ is more prominent on the TP than on VP, as can be seen in Figs. 9a and 9b. When $\gamma > 0$, representing a heat source, TP increases because additional heat is introduced into the fluid, increases the temperature within the boundary layer, and thickens the TBL. Conversely, for $\gamma < 0$, indicating a heat sink, the temperature profile declines as heat is removed from the fluid, leading to a thinner TBL.

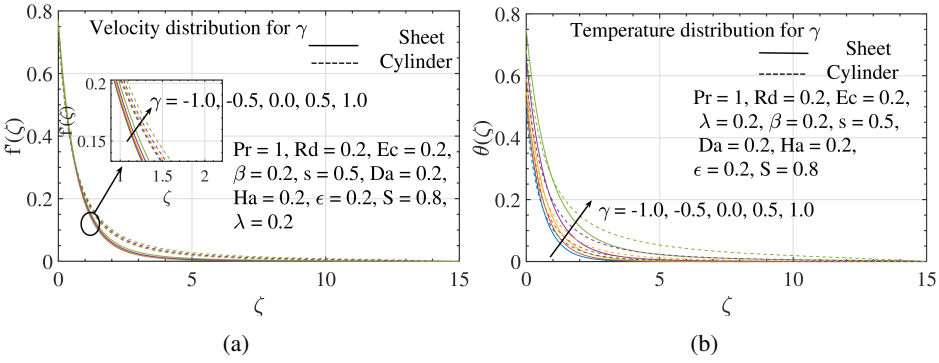

Fig. 9. Impact on (a) velocity and (b) temperature with ζ for different γ

The thermal conductivity parameter ϵ has a negligible effect on VP but significantly affects TP, shown in Fig. 10. Near the surface, the temperature decreases with increasing ϵ due to more efficient heat conduction. However, further into the

boundary layer, the temperature rises as enhanced thermal conductivity of the fluid allows more heat to diffuse into the fluid, thickening the thermal boundary layer.

The thermal radiation parameter *Rd* has a notable impact on TP and Nu_x (see Fig. 11). With increasing *Rd*, the thermal boundary layer thickens, and TP rises as radiative heat transfer intensifies. The radiation effect increases the fluid's internal energy, leading to elevated temperatures within the boundary layer. Also, surface heat transfer rises as the radiation parameter increases, leading to a marked increase in the Nusselt number.

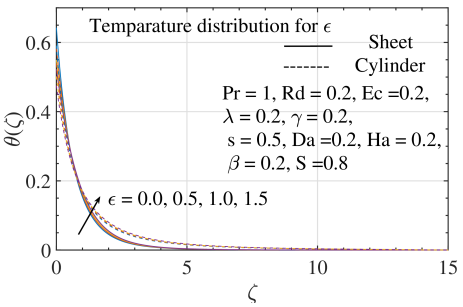

Fig. 10. Impact on temperature with ζ for different ϵ

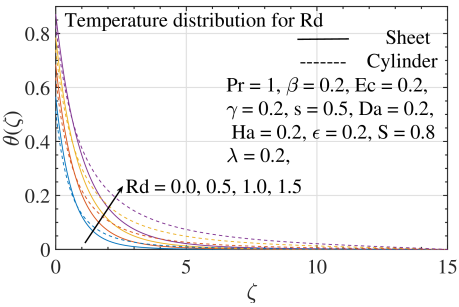

Fig. 11. Impact on temperature with ζ for different *Rd*

Fig. 12 shows the influence of Ec on TP. As Ec increases, the thickness of TBL and the TP also increase significantly. This behavior can be attributed to enhanced viscous dissipation, where kinetic energy from the flow is converted into thermal energy, raising the fluid temperature within the boundary layer. However, this increase in temperature leads to a reduction in the Nusselt number, indicating less efficient heat transfer from the surface to the fluid.

The Prandtl number Pr signifies the relationship between momentum diffusivity and the thermal diffusivity. As shown in Fig. 13, an increase in Pr results in a thinner TBL due to the decreased thermal diffusivity, which slows the rate of

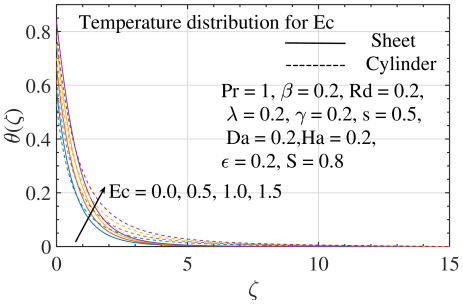

Fig. 12. Impact on temperature with ζ for different Ec

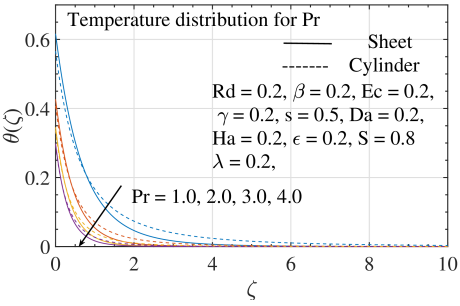

Fig. 13. Impact on temperature with ζ for different Pr

heat diffusion. As a result, TP reduces, keeping the heat concentrated closer to the surface. This behavior enhances the Nusselt number, reflecting more efficient heat transfer from the surface to the fluid.

4.2. Skin-friction coefficient and Nusselt number

The numerical results highlighting the influence of key engineering quantities, namely the skin-friction coefficient ($Cf_x\sqrt{\mathrm{Re}_x}$) and the heat transfer rate ($\mathrm{Nu}_x\mathrm{Re}_x{}^{-0.5}$), are illustrated in Figs. 14–15. The effects of velocity slip parameter (λ) and curvature parameter (δ) on the skin-friction coefficient ($Cf_x\sqrt{\mathrm{Re}_x}$) and Nusselt number ($\mathrm{Nu}_x\mathrm{Re}_x{}^{-0.5}$) are illustrated in Figs. 14a and 14b, respectively. A noticeable reduction in absolute values of $Cf_x\sqrt{\mathrm{Re}_x}$ is observed with increasing λ, indicating that slip at the wall significantly reduces shear stress. In contrast, the influence of δ on skin friction is relatively minor. For heat transfer, $\mathrm{Nu}_x\mathrm{Re}_x{}^{-0.5}$ increases with higher values of δ, confirming the positive role of curvature in enhancing thermal transport, whereas it decreases gradually with increasing λ.

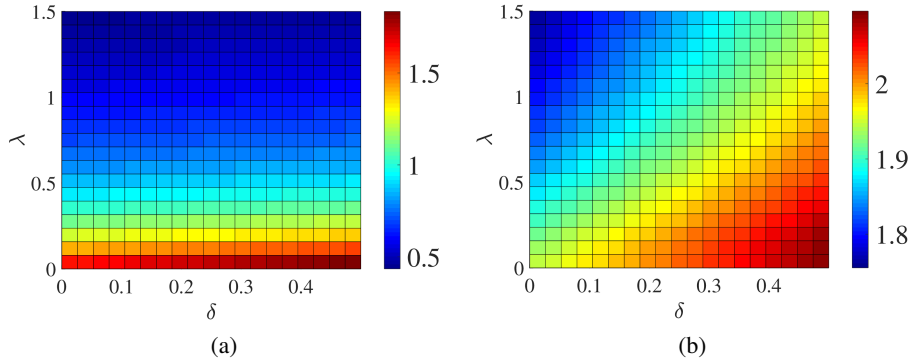

Fig. 14. Variations in (a) $-Cf_x\sqrt{\mathrm{Re}_x}$ and (b) $\mathrm{Nu}_x\mathrm{Re}_x{}^{-0.5}$ with λ and δ

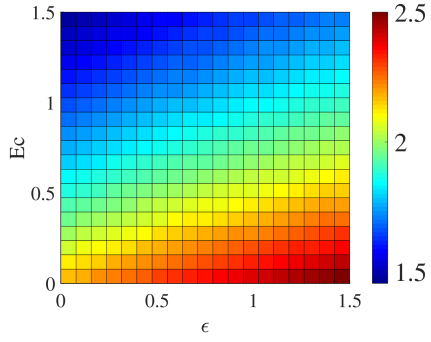

Fig. 15. Variation on $\mathrm{Nu}_x\mathrm{Re}_x{}^{-0.5}$ with ϵ and Ec

Fig. 15 presents the variation in the Nusselt number with thermal conductivity parameter ϵ and Eckert number Ec. It is evident that $\mathrm{Nu}_x\mathrm{Re}_x{}^{-0.5}$ increases with ϵ, indicating enhanced heat transfer. However, increasing Ec leads to a reduction in $\mathrm{Nu}_x\mathrm{Re}_x{}^{-0.5}$, which reflects the adverse effect of viscous dissipation that raises the internal energy of the fluid and lowers the effectiveness of surface heat transfer.

5. Conclusions

This study analyzed the unsteady, axisymmetric, 2-D boundary layer flow of a viscous, electrically conducting fluid over a permeable stretching cylinder, contrasting it with a stretching sheet. The research accounted for complexities like porous medium effects, variable thermal conductivity, heat flux, and the influence of viscous dissipation, thermal radiation, Joule heating, and slip velocity. Using the Bvp4c MATLAB method to solve the derived nonlinear differential equations, this investigation highlights the significant role of curvature on thermal and flow properties, particularly for the stretching cylinder. Key findings are as follows:

1. The stretching cylinder develops thicker MBL and TBL, along with higher skin-friction coefficient and Nusselt number, compared to a flat surface. This is useful in cylindrical heat exchangers and extrusion systems.
2. The parameters β, λ, s, Da, and Ha significantly influence the VP. Specifically, $f'(\zeta)$ increases with β, but decreases with λ, s, Da, and Ha.
3. The dimensionless TP $\theta(\zeta)$ is strongly affected by S, λ, Rd, s, γ, and Ec; it rises with increasing λ, γ, Rd, and Ec, while it declines with higher values of S and s.
4. Increasing ϵ enhances thermal conductivity, which results in a thicker TBL and greater heat transfer rate. This behavior is applicable in cooling technologies involving nanofluids, particularly in curved geometries such as cylindrical heat exchangers, microchannels, or heat pipes, where efficient thermal regulation is critical.
5. The skin friction coefficient decreases with increasing λ, while the Nusselt number reduces with higher λ and Ec, but rises as ϵ increases. These trends are relevant in industrial processes such as wire coating, polymer extrusion over heated cylinders, and thermal surface treatment, where control of surface drag and heat transfer rate is essential for product quality and process efficiency.

Acknowledgements

Department of Mathematics, University of Rajasthan, Jaipur, Rajasthan, India.

References

[1] L.J. Crane. Flow past a stretching plate. *Zeitschrift für angewandte Mathematik und Physik ZAMP*, 21:645–647, 1970. doi: 10.1007/BF01587695.

[2] Ch.Y. Wang. Fluid flow due to a stretching cylinder. *Physics of Fluids*, 31(3):466–468, 1988. doi: 10.1063/1.866827.

[3] A. Ishak, R. Nazar, and I. Pop. Magnetohydrodynamic (MHD) flow and heat transfer due to a stretching cylinder. *Energy Conversion and Management*, 49(11):3265–3269, 2008. doi: 10.1016/j.enconman.2007.11.013.

[4] A. Ishak, R. Nazar, and I. Pop. Uniform suction/blowing effect on flow and heat transfer due to a stretching cylinder. *Applied Mathematical Modelling*, 32(10):2059–2066, 2008. doi: 10.1016/j.apm.2007.06.036.

[5] S. Mukhopadhyay and R.S.R. Gorla. Slip effects on boundary layer flow and heat transfer along a stretching cylinder. 18(2):447–459, 2013. doi: 10.2478/ijame-2013-0026 .

[6] K. Vajravelu, K.V. Prasad, S.R. Santhi, and V. Umesh. Fluid flow and heat transfer over a permeable stretching cylinder. *Journal of Applied Fluid Mechanics*, 7(1):111–120, 2014. doi: 10.36884/jafm.7.01.21135.

[7] S. Munawar, A. Mehmood, and A. Ali. Time-dependent flow and heat transfer over a stretching cylinder. *Chinese Journal of Physics*, 50(5):828–848, 2012.

[8] V. Poply, P. Singh, and K.K. Chaudhary. Analysis of laminar boundary layer flow along a stretching cylinder in the presence of thermal radiation. *WSEAS Transactions on Fluid Mechanics*, 8(4):159–164, 2013.

[9] A. Mahdy. Viscous and joule heating effects on flow heat and mass transfer due to a stretching cylinder with suction/injection. *Journal of Computational and Theoretical Nanoscience*, 10(9):2094–2101, 2013. doi: 10.1166/jctn.2013.3173.

[10] S. Mukhopadhyay and A. Ishak. Mixed convection flow along a stretching cylinder in a thermally stratified medium. *Journal of Applied Mathematics*, 2012(1):491695, 2012. doi: 10.1155/2012/491695.

[11] S. Mukhopadhyay. MHD boundary layer slip flow along a stretching cylinder. *Ain Shams Engineering Journal*, 4(2):317–324, 2013. doi: 10.1016/j.asej.2012.07.003.

[12] E.M.A. Elbashbeshy, T.G. Emam, M.S. El-Azab, and K.M. Abdelgaber. Effect of magnetic field on flow and heat transfer over a stretching horizontal cylinder in the presence of a heat source/sink with suction/injection. *Journal of Applied Mechanical Engineering*, 1(1):1–5, 2012.

[13] B.K. Swain, B.C. Parida, S. Kar, and N. Senapati. Viscous dissipation and joule heating effect on MHD flow and heat transfer past a stretching sheet embedded in a porous medium. *Heliyon*, 6(10):e05338, 2020. doi: 10.1016/j.heliyon.2020.e05338.

[14] P. Kumar, R.S. Yadav, and O.D. Makinde. Numerical study of Williamson fluid flow and heat transfer over a permeable stretching cylinder with the effects of joule heating and heat generation/absorption. *Heat Transfer*, 52(4):3372–3388, 2023. doi: 10.1002/htj.22832.

[15] S. Sinha, M.K. Nahlia, and R.D. Mahla. Viscous dissipation and joule heating effect on MHD boundary layer flow of chemically reactive Jeffrey fluid past a wedge. *ZAMM-Journal of Applied Mathematics and Mechanics/Zeitschrift für Angewandte Mathematik und Mechanik*, 105(5):e70100, 2025. doi: 10.1002/zamm.70100.

[16] M.I. Khan, M. Tamoor, T. Hayat, and A. Alsaedi. MHD boundary layer thermal slip flow by nonlinearly stretching cylinder with suction/blowing and radiation. *Results in Physics*, 7:1207–1211, 2017. doi: 10.1016/j.rinp.2017.03.009.

[17] A.M. Megahed, M.G. Reddy, and W. Abbas. Modeling of MHD fluid flow over an unsteady stretching sheet with thermal radiation, variable fluid properties and heat flux. *Mathematics and Computers in Simulation*, 185:583–593, 2021. doi: 10.1016/j.matcom.2021.01.011.

[18] Z. Khan, M. Jawad, E. Bonyah, N. Khan, and R. Jan. Magnetohydrodynamic thin film flow through a porous stretching sheet with the impact of thermal radiation and viscous dissipation. *Mathematical Problems in Engineering*, 2022(1):1086847, 2022. doi: 10.1155/2022/1086847.

[19] M. Qayyum, S. Afzal, M.R. Ali, M. Sohail, N. Imran, and G. Chambashi. Unsteady hybrid nanofluid (UO 2, MWCNTs/blood) flow between two rotating stretchable disks with chemical reaction and activation energy under the influence of convective boundaries. *Scientific Reports*, 13(1):6151, 2023. doi: 10.1038/s41598-023-32606-4.

[20] A.M. Megahed. Carreau fluid flow due to nonlinearly stretching sheet with thermal radiation, heat flux, and variable conductivity. *Applied Mathematics and Mechanics*, 40(11):1615–1624, 2019. doi: 10.1007/s10483-019-2534-6.

[21] F. Waseem, M. Sohail, N. Sarhan, E.M. Awwad, and M.J. Khan. Utilization of OHAM to investigate entropy generation with a temperature-dependent thermal conductivity model in hybrid nanofluid using the radiation phenomenon. *Open Physics*, 22(1):20240059, 2024. doi: 10.1515/phys-2024-0059.

[22] P. Sreenivasulu, N. Bhaskar Reddy, and T. Poornima. Variable thermal conductivity influence on hydromagnetic flow past a stretching cylinder in a thermally stratified medium with heat source/sink. *Frontiers in Heat and Mass Transfer (FHMT)*, 9(1):1–7, 2017. doi: 10.5098/hmt.9.20.

[23] S. Rehman, M. Idrees, R.A. Shah, and Z. Khan. Suction/injection effects on an unsteady MHD Casson thin film flow with slip and uniform thickness over a stretching sheet along variable flow properties. *Boundary Value Problems*, 2019:26, 2019. doi: 10.1186/s13661-019-1133-0.

[24] D. Dey, R. Borah, and B. Mahanta. Boundary layer flow and its dual solutions over a stretching cylinder: stability analysis. In *Emerging Technologies in Data Mining and Information Security: Proceedings of IEMIS 2020, Volume 1*, pages 27–38. Springer, 2021. doi: 10.1007/978-981-15-9927-9_3.

[25] R. Raza, M. Sohail, T. Abdeljawad, R. Naz, and P. Thounthong. Exploration of temperature-dependent thermal conductivity and diffusion coefficient for thermal and mass transportation in sutterby nanofluid model over a stretching cylinder. *Complexity*, 2021(1):6252864, 2021. doi: 10.1155/2021/6252864.

[26] Adebayo Stephen Oladoja, Damilare John Samuel, and Yusuf Buba Chukkol. Variable thermophysical property and ohmic heating impact on radiative Casson fluid flow past a stretching cylinder. *FUDMA Journal of Sciences*, 9(5):155–163, 2025. doi: 10.33003/fjs-2025-0905-3476.

[27] W. Ibrahim and M. Negera. Viscous dissipation effect on mixed convective heat transfer of MHD flow of Williamson nanofluid over a stretching cylinder in the presence of variable thermal conductivity and chemical reaction. *Heat Transfer*, 50(3):2427–2453, 2021. doi: 10.1002/htj.21985.

[28] M.A. Ismail, N.F. Mohamad, M.R. Ilias, and S. Shafie. MHD effect on unsteady mixed convection boundary layer flow past a circular cylinder with constant wall temperature. In *Journal of Physics: Conference Series*, volume 890, page 012054. IOP Publishing, 2017. doi: 10.1088/1742-6596/890/1/012054.

[29] Y.J. Lim, S. Shafie, S.M. Isa, N.A. Rawi, and A.Q. Mohamad. Impact of chemical reaction, thermal radiation and porosity on free convection carreau fluid flow towards a stretching cylinder. *Alexandria Engineering Journal*, 61(6):4701–4717, 2022. doi: 10.1016/j.aej.2021.10.023.

[30] S.T. Abbas, E. Rafique, I. Haider, and M. Sohail. Utilization of OHAM on mixed convective flow of Williamson fluid model with viscous dissipation over a stretched cylinder. *UNEC Journal of Engineering and Applied Sciences*, 4(1):20–36, 2024. doi: 10.61640/ujeas.2024.0502.

[31] M. Tamoor. MHD convective boundary layer slip flow and heat transfer over nonlinearly stretching cylinder embedded in a thermally stratified medium. *Results in Physics*, 7:4247–4252, 2017. doi: 10.1016/j.rinp.2017.07.064.

[32] S. Das, R.N. Jana, and O.D. Makinde. Slip flow and radiative heat transfer on a convectively heated vertical cylinder. *Journal of Engineering Physics and Thermophysics*, 90:568–574, 2017. doi: 10.1007/s10891-017-1602-1.

[33] S. Bansal and R.S. Yadav. Effect of slip velocity on newtonian fluid flow induced by a stretching surface within a porous medium. *Journal of Engineering and Applied Science*, 71(1):153, 2024. doi: 10.1186/s44147-024-00481-z.

[34] M.M. Nandeppanavar, M.C. Kemparaju, R. Madhusudhan, and S. Vaishali. MHD slip flow and convective heat transfer due to a moving plate with effects of variable viscosity and thermal conductivity. *Multidiscipline Modeling in Materials and Structures*, 16(5):991–1018, 2020. doi: 10.1108/MMMS-08-2019-0142 .

[35] A. Cham and M. Mustafa. Boundary layer formations over a stretchable heated cylinder in a viscoelastic fluid with partial slip and viscous dissipation effects. *Numerical Heat Transfer, Part A: Applications*, 85(11):1767–1779, 2024. doi: 10.1080/10407782.2023.2210259.

[36] I. Ullah, T.A. Alkanhal, S. Shafie, K.S. Nisar, I. Khan, and O.D. Makinde. MHD slip flow of Casson fluid along a nonlinear permeable stretching cylinder saturated in a porous medium with chemical reaction, viscous dissipation, and heat generation/absorption. *Symmetry*, 11(4):531, 2019. doi: 10.3390/sym11040531.

[37] S. Sadighi, H. Afshar, H.A.D. Ashtiani, and M. Jabbari. MHD flow and conductive heat transfer on a permeable stretching cylinder: Benchmark solutions. *Case Studies in Thermal Engineering*, 44:102886, 2023. doi: 10.1016/j.csite.2023.102886.

[38] Y.D. Reddy, B.S. Goud, K.S. Nisar, B. Alshahrani, M. Mahmoud, and C. Park. Heat absorption/generation effect on MHD heat transfer fluid flow along a stretching cylinder with a porous medium. *Alexandria Engineering Journal*, 64:659–666, 2023. doi: 10.1016/j.aej.2022.08.049.

[39] V. Vinita and V. Poply. Impact of outer velocity MHD slip flow and heat transfer of nanofluid past a stretching cylinder. *Materials Today: Proceedings*, 26:3429–3435, 2020. doi: 10.1016/j.matpr.2019.11.304.

[40] A. Majeed, T. Javed, and S. Shami. Numerical analysis of Walters-B fluid flow and heat transfer over a stretching cylinder. *Canadian Journal of Physics*, 94(5):522–530, 2016. doi: 10.1139/cjp-2015-0511.

[41] S. Dey, S. Mukhopadhyay, and K. Vajravelu. MHD nanofluid flow and heat transfer past a horizontal stretching cylinder in darcy porous medium in presence of slip and uniform/variable wall temperature. *Journal of Computational Applied Mechanics*, 56(2):380–395, 2025. doi: 10.22059/jcamech.2025.388665.1336.

[42] P.M. Patil, S. Roy, and I. Pop. Unsteady effects on mixed convection boundary layer flow from a permeable slender cylinder due to non-linearly power law stretching. *Computers & Fluids*, 56:17–23, 2012. doi: 10.1016/j.compfluid.2011.11.008.

[43] K.V. Prasad, K. Vajravelu, P.S. Datti, and B.T. Raju. MHD flow and heat transfer in a power-law liquid film at a porous surface in the presence of thermal radiation. *Journal of Applied Fluid Mechanics*, 6(3):385–395, 2013. doi: 10.36884/jafm.6.03.19563.